Study on Sediment Movement over Type-A Piano Key Weirs

Binit Kumar[1]; Subhojit Kadia[2]; and Zulfequar Ahmad[3]

[1]Research Scholar, Department of Civil Engineering, Indian Institute of Technology Roorkee, Uttarakhand 247667, India, Email: binit.nit2010@gmail.com, Mobile: +919709408849, ORCID ID 0000-0002-3911-7105 (**Corresponding author**)

[2]M. Tech., Department of Water Resources Development and Management, Indian Institute of Technology Roorkee, Uttarakhand 247667, India, Email: subhojitkadia@gmail.com, ORCID ID 0000-0002-9134-3222

[3]Professor, Department of Civil Engineering, Indian Institute of Technology Roorkee, Uttarakhand 247667, India, Email: zulfifce@iitr.ac.in

Abstract

This investigation deals with the mechanics of movement of singular quartz gravel and coarse sand river bed particles in upstream and over inlet key of three type-A Piano key weir (PKW) models, which were recorded with a high-speed camera. Acoustic-Doppler-Velocimeter was used to obtain the upstream bed shear stress. The sediment threshold and regime over the upstream bed were compared with the previous investigations and found to be within the ranges. Generally, a sediment particle decelerates as it approaches the inlet key, but accelerates over it due to flow contraction and an increase in shear stress. Rolling and saltation regimes were observed over the key. The maximum particle velocity at the key end was higher in case of 1-cycle model than 2-cycles than 3-cycles. CFD simulation shows a rapid increase in shear stress at the key end. For the used models, PKW required 17%–43% of additional shear stress on the upstream bed to pass sediment over the key. This study is useful for the in-channel application of PKW and sediment flushing over it.

Keywords: Sediment movement; Particle tracking; Piano key weir; High-speed camera; CFD.

Introduction

Piano key weir (PKW) has a greater discharging capacity than other weirs and has been constructed widely in recent times not just as dam spillway but also in large diversion projects in Vietnam and

India (Ho Ta Khanh 2017; Das Singhal and Sharma 2011). A three-cycles type-A PKW configuration with noses beneath the upstream apexes is shown in Fig. 1(a). Where *a* and *b* are inlet and outlet keys widths; *P* is the key height; B_i and B_o are inlet and outlet keys overhangs; *W* is the width of the channel; and other terms are described in notations. Noses below the upstream apexes reduce the inlet energy loss and provide a better flow condition at the inlet entrance (Anderson and Tullis 2013). However, the construction of a transverse hydraulic structure leads to increase in the upstream flow depth and reduction in flow velocity which results into non-uniformity in flow and sediment discontinuity (Bai and Duan 2014; Fan and Morris 1992; Tiwari and Sharma 2015). This may further deposits sediment in the backwater or transports it to the weir during the heavy flood events, thus hampering the channel navigation and may result in upstream inundation (Noseda et al. 2019).

The investigations on the complexity of sediment movement caused by the streamflow in the watercourse were given utmost importance since the 1st half of the 20th century. Perhaps, Shields (1936) initiated the study on the incipient movement of non-cohesive sediments in alluvial bed. The primary governing factors for the sediment transport are the fluid, flow and sediment characteristics (Garde and Albertson 1959; Garde and Ranga Raju 2015). However, the threshold condition for particle motion on a smooth bed is inferior to that for alluvial bed and the Shields method overestimates the critical condition for smooth bed (Bridge and Dominic 1984; Novak and Nalluri 1975, 1984; Ramesh et al. 2011; Safari et al. 2017).

Earlier experimental investigations and Computational Fluid Dynamics (CFD) simulations on PKW dealt predominantly with its discharging capacity, the influence of different geometric parameters, design guidelines, construction strategies and case studies while focusing mainly on the impact of tailwater submergence, aeration, floating debris, energy dissipation, scale effects, cost involvement etc. as reported in several review studies by Abhash and Pandey (2020); Crookston et al. (2019); Erpicum et al. (2017); Oertel (2018), but it appears that a very limited study (possibly the only one by Noseda et al. (2019)) has been performed on the sediment movement over PKW. The previous investigations by Sharma and Tiwari (2013); Tiwari and Sharma (2015) were mainly based on visual observations and limited to suspended load transport and threshold of the lifting of sediment upto 2 mm. Noseda et al. (2019) carried out an experimental study on the self-cleaning capacity of PKW and examined the upstream riverbed scour behavior and flushing of sediments over the weir. A comparison between the investigations conducted by Noseda et al. (2019) and Gebhardt et al. (2019) indicates the superior self-cleaning capacity of PKW than rectangular labyrinth weir. Hence, the main governing factor behind such observations is the slopping inlet key. The downstream scouring has been studied by Jüstrich et al. (2016); Kumar and Ahmad (2020), and it is directly affected by the residual energy which has been studied by Eslinger and Crookston (2020); Silvestri et al. (2013). CFD simulation has also been used by several researchers to study different aspects related to PKW. Crookston et al. (2018) performed 40 simulations and validated the results with previous experimental data and suggested empirical equations for estimation of the coefficient of discharge of type-A PKW. Hu et al. (2018) studied the discharge passing contributions of upstream crest, downstream crest and sidewall crest and found that the contribution of sidewall crest reduces with an increase in the tailwater depth. Denys and Basson (2020) studied the unsteady hydrodynamic forces present around the PKW and found that the vortices in the inlet key are the significant source of excitations and expose the sidewall to episodic fluctuations of pressure.

The sediment movement over a PKW is a complex and interesting phenomenon and attracts micro-level investigations. Several studies have been carried out formerly to analyze the behavior of particle movement over fixed and mobile beds. The bed load particles can travel in three regimes namely sliding or transition, rolling and saltation depending on the Shields number N_{sh} (or Shields parameter) which is determined as the ratio of the bed shear stress to the stress imposed by the buoyant weight of particle (Ancey et al. 2002; Ramesh et al. 2011). Shields number is expressed as $N_{sh} = (\boldsymbol{u_c}^*)^2/(S_s - 1)\text{g}d$, where $\boldsymbol{u_c}^*$ is the critical shear velocity in m/s, S_s is the specific gravity of sediment, g is the acceleration due to gravity in m/s^2 and d is particle size in m. For a gently sloped bed, the transition, rolling and saltation regimes attain at N_{sh} ranges 0.001 – 0.005, 0.005 – 0.01 and > 0.3, respectively as suggested by Ancey et al. (2002). Table 1 shows contributions of some of the major experimental studies carried out on particle tracking during its movement over a fixed bed. In addition to those experimental studies, Bridge and Dominic (1984) suggested empirical equations to estimate the mean particle velocity in saltation regime and bed load transport rate. The velocity of a particle moving over a fixed rough bed and bed load transport rate for plane bed experimental results can be accurately estimated using those equations. Subsequently, Wiberg and Smith (1985) proposed a mathematical model to predict the trajectory of individual particles in saltation and rolling modes and to determine the mean particle velocity, whereas Niño and García (1994) proposed another model for coarse gravel particles.

In the case of the alluvial bed, the particle movement also depends on the roughness created by the bed particles and the variation in the bed-forms (Tregnaghi et al. 2012). The study on the particle motion characteristics during its movement over the mobile bed was conducted out by Fernandez Luque and Van Beek (1976); Niño et al. (1994); Lee and Hsu (1994); Shim and Duan (2017); Shim and Duan (2019) using standard video-imaging technique, real-time flow visualization technique, continuous tracking record and VIPT (video image-based particle tracking technique) software. Recently, Zhao et al. (2020) found an increase in the saltation height and length if the particle shape is not spherical.

It is observed that limited detailed studies have been carried out on the sediment movement over weir structures. The complexity of flow around PKW and its effect on the particle movement make the study more interesting. Therefore, the present systematic investigation was initiated to have an insight into the particle motion characteristics over PKWs and their correlation with particle size and flow parameters. The study focuses on the incipient movement of singular sediment particles (quartz gravel and coarse sand) ranging from 1.7 to 6.3 mm (a total of 12 sizes) during their movement over the smooth upstream bed and inlet key of three type-A PKW models through tracking of such motions using a high-speed camera and image processing technique. An Acoustic Doppler Velocimeter (ADV) was used to determine the shear stress on the upstream bed, and Computational fluid dynamics (CFD) simulation was performed to relate the particle kinematics with the shear stress and maximum flow velocity over the key. This study is going be a substantial addition to the recent developments on PKW and will be very useful in planning and designing of PKW keeping in view the problem of upstream sedimentation.

Experimental set-up

Three PKW models namely PK_1 (1-cycle), PK_2 (2-cycles) and PK_3 (3-cycles) and twelve sediment sizes were considered in this study. The geometrical configurations of the models are listed in Table 2. All experiments were performed in the Hydraulic Engineering Laboratory at IIT Roorkee in a 15.0 m long, 0.39 m wide and 0.5 m deep flume. The models which are shown in Fig. 1(b) were fabricated with 0.006 m thick acrylic sheet. The noses beneath the outlet apexes were projected upto half of the outlet overhangs, $B_o/2$ = 0.032 m. The flume has glass-walled in its major portion for proper visualization of flow and was fed from an inlet pipe of 0.1 m diameter. An advanced, precise, pre-calibrated ultrasonic flowmeter having an accuracy of ±1% was used to measure the discharge values. The flow depth was measured using a point gauge (with Vernier scale) having least count of 0.0001 m only and the least count of the ADV measurement was 0.0001 m/s only. The maximum experimental uncertainty was found to be about 1.2% only. Two honeycomb grid walls, a series of flow straighteners and wave suppressor were placed upstream of the flume to minimize surface disturbance and cross-currents. A high-speed digital camera (IPX-VGA210L) capable of recording at 207 FPS was placed at the right side of the flume and connected to a workstation PC for storage and further processing of the recordings. Proper illumination was maintained using a LED bulb. Better visualization was ascertained by coloring particles (red) and upstream bed (white). Further, a 10 MHz Vectrino ADV was used to measure the instantaneous velocity of flow along the depth. The measured velocity profiles were used to calculate the shear stress on the upstream smooth bed. The schematic diagram of the experimental set-up is shown in Fig. 1(c). Figures 2(a) and 2(b) show the examples of video recording and velocity measurement, respectively.

Methodology

Video recording, image analysis and sediment tracking

Each of the twelve individual sediments fed manually inside the flume at a distance about 1.8 m upstream of the PKW. Non-cohesive river bed sediments (nearly rounded) comprising quartz coarse sand and quartz gravel particles were used in the study. The specific gravity was found to be 2.64. For each combination of sediment and PKW model, the test was started at a lower discharge and increased gradually with small increments of 0.1–0.2 × 10^{-3} m^3/s till the sediment starts moving over the inlet key bed. For 1.7 mm particle moved over the inlet key of PK_3 model, the discharge and total head over the weir crest were 13.55 × 10^{-3} m^3/s and 0.0323 m, respectively. Video recording was started immediately when the sediment approached near the field of recording. The field was 325 mm long and 247.5 mm deep, whereas the resolution of recording was 320 pixels × 480 pixels. The length and height of each pixel were 1.0156 mm and 0.5156 mm, respectively. At first, the camera captured videos at 207 FPS and the continuous footages were stored using STREAMPIX software and frame grabber card. Each recording was processed in STREAMPIX software and converted into a series of image sequences. The positions of sediment at different time steps were obtained from these image sequences using IMAGE-PRO PLUS software. However, those positions were available in terms of pixel values and the origin (0,0) of the pixel grid was located at the top left corner of the image. The positions were converted into a 2D Cartesian coordinate system using the pixel dimensions and considering the inlet entrance as the origin (0,0). Figure 3 shows the pixel and Cartesian coordinate systems, images of sediment moving on the upstream bed and inlet key bed and its distance from the origin, i.e. L_k. For a better representation of the large variation in particle velocity observed along its route of movement, the particle tracking was done by taking time steps of 20 frames in the upstream channel bed (deceleration segment), upstream part of inlet key (transition segment) and 10 frames in the remaining inlet part (accelerating segment). The recordings were processed for those events only in which sediment moved over the rightmost half inlet key and there was no visual obstruction due to the PKW sidewalls. In these events, it was observed that sediment passes in the key along a longitudinal plane located close to the flume's right boundary. The pixel calibration and camera focusing were done on that boundary. The effect of 2D imaging and perspective distortion was negligible.

Mechanics of a particle motion

Once the tracked positions of a particle are available at different time steps, the method suggested by Mazumder et al. (2008); Ramesh et al. (2011) was utilized to determine the instantaneous particle motion characteristics. Following the forward difference technique and using the consecutive positions of a particle at different time steps, particle kinematics and dynamics parameters were determined.

Shear stress on the upstream channel bed

The shear stress on the upstream smooth channel bed was obtained at a location of 0.1235 m upstream of the outlet key by observing the velocity profile over the bed using ADV and fitting it in the well-known Prandtl-Karman logarithmic equation available for smooth bed (Carvalho et al. 2010; Ferro 2003; Kumar et al. 2019; Ramesh et al. 2011). For each point, the mean flow velocity was obtained from the filtered data separated from 3000 raw samples (60 seconds of recording at 50 Hz) of instantaneous velocity. The data filtration was processed in Explorer V software by fixing the minimum correlation (COR) to 70 and minimum signal-to-noise-ratio (SNR) to 15 (Kumar et al. 2019; Sharma and Tiwari 2013; Voulgaris and Trowbridge 1998). The depth of flow, y was measured at 0.5 m upstream of the outlet key.

Shear stress on the inlet key

The velocity profile over the inlet key could not be measured precisely, probably due to flow complexity, high turbulence, unsteadiness of flow and vortices within inlet key as observed by Denys and Basson (2020) and flow separation at the tip of the sensor. So, the shear stress on the inlet key bed could not be determined experimentally and was obtained from CFD simulation performed in ANSYS 19.1 academic software (ANSYS 2018). It was then correlated with the particle kinematics. For convenience, the force balancing method suggested by Wiberg and Smith (1985); Chiew and Parker (1994) for a sediment particle resting on a sloping surface was utilized to balance the forces acting on a sediment particle moving over the inlet key bed of PKW.

The resultant effective force on the particle = total hydrodynamic force exerted by the moving water on the particle – the tangential weight component of the particle – resistance imposed by bed friction; i.e.,

$$\boldsymbol{F_s} = \boldsymbol{F_t} - \boldsymbol{W}' \sin\boldsymbol{\alpha} - \boldsymbol{W}' \mu \cos\boldsymbol{\alpha} \tag{1}$$

where $\boldsymbol{F_s}$ is the effective hydrodynamic force causing sediment movement, which is the product of the mass of the particle and its acceleration $\boldsymbol{a_s}$ in submerged condition; $\boldsymbol{F_t}$ is the total/gross force acting on the particle as a combination of hydrodynamic drag, lift and basset force; A is the projected area of the particle on which the fluid force is acting; $\boldsymbol{W'}$ is the submerged weight of particle; $\boldsymbol{\alpha}$ is the inclination of the inlet key and μ is the friction coefficient. Both the drag and lift forces are functions of the characteristics velocity of flow which further depends on the shear velocity (Chiew and Parker 1994; Garde and Ranga Raju 2015). Therefore, $\boldsymbol{F_t}$ is directly related to the bed shear stress imposed on the inlet key bed $\boldsymbol{\tau_o}$. Here, the variation in the basset force or history force which could occur because of the variation in the relative motion of sediment and water is neglected because the estimation of such variation within the inlet key of PKW where accurate measurement of the flow properties is challenging becomes very difficult. It has been observed that researchers have previously neglected the basset force in numerical modeling (Bombardelli et al. 2008; Lee and Hsu 1994; Moreno-Casas and Bombardelli 2016; Rostami et al. 2006; Schmeeckle and Nelson 2003). However, the basset force becomes an important factor for small sand particles moving in a flow having a relatively low Reynolds number. Niño and García (1998a) found that the effect of the basset force is significant for small sand particles having the explicit particle Reynolds number $\mathrm{R_p} = ((S_s - 1)\mathrm{g}d^3)^{0.5}/\nu$ from 50 to 100 but not so substantial for $\mathrm{R_p} \geq 500$. In the present study, gravel and coarse sand particles were used and $\mathrm{R_p}$ varied from 315 to 2247. Therefore, it can be assumed that the basset force is not so significant. The accurate estimation of the drag and lift components is difficult, and therefore, an attempt was made to understand the trend of particle acceleration varying with the shear stress $\boldsymbol{\tau_o}$. For a particle of size d, let us assume that A, $\boldsymbol{W'}$, $\boldsymbol{\alpha}$ and μ are constant along its path of movement. Therefore, it can be considered that $\boldsymbol{a_s} = f(\boldsymbol{\tau_o})$, where f is a function. However, in the actual scenario, this assumption may not always be entirely accurate because of the variation in the projected area of particle and μ during rolling and saltation regimes, unsteadiness in the flow characteristics, the effect of the basset force for smaller particles and the spatially varied nature of flow along the inlet key.

CFD simulation

The CFD simulations were carried out using CFX solver which requires less computational cost and space than Fluent solver due to a lesser number of degrees of freedom (Berggren et al. 2009; Kadia et al. 2020). The widely used standard k-ε turbulent model (an eddy-viscosity model) which was introduced by Launder and Spalding (1972, 1974) was used in the present simulation. The simulation was carried out at a discharge of 19.7×10^{-3} m^3/s for all three PKW models following the method available in the literature (Kadia et al. 2020). A 1.5 m long domain having cross-sections 0.39 m × 0.335 m in the downstream side and 0.39 m × 0.3 m in the upstream side was modeled. The meshing was finalized with the tetrahedron method considering 0.00709 m size of bed faces and fixing the maximum size of the element at 0.0156 m. A total of about 0.7 to 0.8 million small elements were created. As the near-bed flow properties are very crucial in estimating the velocity gradient and bed shear stress, 5 to 10 inflation layers were created near the bed for better representation of the flow. The total simulation time and time steps were selected as 30 s and 0.05 s, respectively. Multiphase (water as primary phase) and open channel modules were considered. A transient flow simulation of the domain was initialized considering mean velocity on the inlet face. A pressure-based outlet was considered and the top opening of the domain was configured with relative pressure normal to the plane. The boundary conditions for PK_3 model simulation are shown in Fig. 4. The simulation was based on the Volume of Fluid (VOF) method and the finite volume technique.

Results and discussion

Particle movement, kinematics and dynamics

PKW has an impact on flow and sediment continuity of a channel, just like other similar hydraulic structures, but it has the self-cleaning capability. While observing the sediment movements over the inlet keys of PKW, it was found that sediment moves along the centre of a full inlet key and close to the sidewall in case of half key for which the tracking was done. The sediment movement in the approaching segment, i.e. in the upstream of an inlet key was found to be 3D, but due to the limitation of 2D tracking the lateral component of the particle movement could not be measured. A total of thirty-six image sequences were analyzed for particle motion characteristics and two of them are shown in Fig. 5. In general, and as shown in Fig. 6, it was observed that sediment tends to slow down while approaching the inlet key. For larger particles, and especially in case of PK_1, the transition segment along the path of movement was observed. The slight movements in the upstream part of the key in these cases may look similar to what was observed earlier by Kumar et al. (2019) for sediment movement over a ramp. But still, these movements are faster than what was observed for the ramp. Except for those few cases, particle starts accelerating immediately after reaching near the inlet key entrance and there was no transition segment in its path of movement. The possible reason is the formation of accelerating flow pattern near the inlet key caused by the contractions in both vertical and lateral directions as observed by Denys and Basson (2020).

Figures 6(a–c) show the variation in particle velocity $\boldsymbol{v_s}$, particle acceleration $\boldsymbol{a_s}$, angle of orientation of the velocity vector $\boldsymbol{\theta_s}$ and applied force on the sediment $\boldsymbol{F_s}$ for 4.05 mm particle travelling over the three PKW models. The required discharge values to pass 4.05 mm particle over the inlet key bed of PK_1, PK_2 and PK_3 were 22.0×10^{-3}, 18.65×10^{-3} and 18.2×10^{-3} m^3/s, respectively, which indicate a considerable variation in the flow characteristics depending on the PKW configuration. There is a contraction of flow area within the key along the flow direction, and it was found that particle accelerates rapidly in the upstream part and downstream end of the key as shown in Figs. 6(a–b). Such variations in $\boldsymbol{v_s}$, $\boldsymbol{a_s}$ are affected by the changes in inlet key shear stress ($\boldsymbol{\tau_o}$) (obtained from the CFD simulations and discussed later), high turbulence, unsteadiness of flow within the inlet key as indicated by Denys and Basson (2020) and changes in the projected area of the particle during rolling and saltation regimes. Therefore, no smooth pattern of variations was found. The sediment generally accelerated in the rising part of a saltation event and decelerated in its falling part. The maximum observed $\boldsymbol{v_s}$ in the study was 0.617, 0.609 and 0.458 m/s for PK_1, PK_2 and PK_3, respectively. Generally, for all d the highest $\boldsymbol{v_s}$, $\boldsymbol{a_s}$ and $\boldsymbol{F_s}$ were witnessed for PK_1 model having a wider inlet key and which requires higher discharge (and a slightly higher approach flow velocity) to pass the same sediment than the other models.

The orientation of the particle velocity vector to the horizontal axis ($\boldsymbol{\theta_s}$) is directly related to the regime of the sediment movement. The fluctuations and maximum values of $\boldsymbol{\theta_s}$ are higher for saltation regime than rolling and sliding. It was found that $\boldsymbol{\theta_s}$ varies from 50.9 to 13.8 degree for particle movement over the inlet key bed. For all three PKWs, the extremum, range and average of $\boldsymbol{\theta_s}$ were determined and plotted against particle size d as shown in Fig. 7. Figure 7(c) indicates that sediment passing PK_1 has a larger range of $\boldsymbol{\theta_s}$ than that of the other two models, and in general, the range increases with a rise in d. The rapid rotation of sediment during rolling and saltation regimes, the jumps during saltation, some irregularity in particle shape and stochastic nature of flow are contributing to the fluctuation of $\boldsymbol{\theta_s}$. Further, the fluctuations in $\boldsymbol{\theta_s}$, $\boldsymbol{v_s}$ and $\boldsymbol{a_s}$ were calculated from their instantaneous and mean values obtained from thirty-six experimental runs (and a total of 665 tracking results) following the method used by Ramesh et al. (2011). The model wise frequency distribution f is shown in Fig. 8, which indicates higher fluctuations in all three parameters for PK_1 than that for other models. The distributions of $\boldsymbol{\theta'_s}$ and $\boldsymbol{a'_s}$ can be approximated to a bell-shaped distribution, but the distribution of $\boldsymbol{v'_s}$ for PK_2 and PK_3 does not follow a similar trend. Ramesh et al. (2011) found a similar kind of distribution trend for particle movement over a transitionally rough bed with a gentle slope. The variations are caused by a collective effect of the interaction between sediment and flow, flow unsteadiness and non-uniformity, particle collision with inlet bed and the spatially varied flow formed due to the flow proportion passing over the sidewalls.

Critical condition and the regime of particle motion

As reported earlier, the critical shear stress for the movement of individual sediment on the smooth bed is much lower than the same for alluvial condition and the difference is lower for small particles. Figure 9 shows the difference between Shields curve plotted from Chien and Wan (1999) and the plots obtained for smooth bed from Novak and Nalluri (1975); Safari et al. (2017) and in the present study. From the study carried out by Novak and Nalluri (1975) in a rectangular channel taking singular particles from 0.6 to 50 mm, N_{sh} can be expressed as:

$$\mathrm{N_{sh}} = \frac{2.03}{\gamma d^{0.6}} \tag{2}$$

where γ is the specific weight of water in N/m^3 and d in m. Later, Safari et al. (2017) suggested Eq. (3) for rectangular cross-sections and it is applicable for low Particle Reynolds numbers ($\mathrm{Re}^* = \boldsymbol{u_c}^* d/\nu$) from 1.4 to 15.51, where $\boldsymbol{u_c}^*$ in m/s, ν is the kinematic viscosity in m^2/s and d in m.

$$\mathrm{N_{sh}} = 0.07\left(\mathrm{Re}^*\right)^{-1.14} \tag{3}$$

The shear stress on the smooth upstream bed was determined for the beginning of sediment movement (i) on the upstream bed ($\boldsymbol{\tau_{cbib}}$) and (ii) on the inlet key ($\boldsymbol{\tau_{cbik}}$) for all thirty-six cases using the measured velocity profiles, and the corresponding Shields number $\mathrm{N_{sh}}$ values were calculated to compare the observed critical condition and particle regime with the previous studies. For the critical motion of a particle on the upstream smooth bed, the particle generally moved in sliding or transition regime and $\mathrm{N_{sh}}$ varied from 0.0029 to 0.0056 which is very close to the range (0.001 to 0.005) suggested by Ancey et al. (2002). Figure 9 shows that the observed critical $\mathrm{N_{sh}}$ values are higher than what was suggested by Safari et al. (2017) but lower than what was determined from Novak and Nalluri (1975). The difference in experimental conditions and the flow alternation caused by PKW may be attributed to such differences. It was found that the lateral and vertical components of the near-bed velocity at the location (0.1235 m upstream of the outlet key) where the velocity profile and shear stress were obtained are about 2–3% of the longitudinal velocity component. These components have slightly influenced such differences. Using the thirty-six observed datasets for critical sediment movement over the smooth upstream bed, the following expression is determined based on regression approach

$$\mathrm{N_{sh}} = 0.015\left(\mathrm{Re}^*\right)^{-0.333} \qquad (R^2 = 0.81) \tag{4}$$

Equation (4) has a coefficient of determination $R^2 = 0.81$, and it is applicable for (i) similar type of smooth bed conditions, (ii) non-cohesive river bed quartz coarse sand and gravel and (iii) $19 \leq \mathrm{Re}^* \leq 125$. Both Fig. 9 and Eq. (4) indicate a decreasing trend of $\mathrm{N_{sh}}$ with an increase in the particle size and particle Reynolds number, which is similar to the observations made by Novak and Nalluri (1975); Safari et al. (2017). Further, while plotting the calculated $\mathrm{N_{sh}}$ against the observed values, it was observed that Eq. (4) underestimates N_{sh} for the datasets collected from previous studies as shown in Fig. 10(a). The mean absolute percentage error values are about 42%, 33.2% and 6.72% for the datasets collected from Novak and Nalluri (1975); Ramesh et al. (2011) and the present study, whereas the maximum absolute percentage error is about 60%. The difference in the experimental conditions and the effect of PKW on the upstream flow condition may be attributed to such deviations. The datasets available in Safari et al. (2017) were not used in this comparison because in those cases $Re^* \leq 19$.

Additional bed shear is required on the upstream smooth bed to move sediment over the inlet key. It is being used to counter the tangential component of particle weight that resists the climbing of the particle. For these cases, the regime of a particle during its movement over the upstream bed and inlet key bed was observed during the particle tracking. The particle regime in upstream of the weir and corresponding observed N_{sh} were compared for the conditions suggested by Ancey et al. (2002). It was found that smaller particles require greater upstream N_{sh} to move over the inlet key bed as compared to larger ones for all three PKWs as shown in Table 3. For larger particles (in eleven cases), the rolling regime was observed over the upstream bed, even though N_{sh} was below 0.005 as shown in Table 3. Whereas, there was no rolling motion in four cases (mostly for PK_3) despite $N_{sh} > 0.005$. These observations differ from the condition suggested by Ancey et al. (2002). However, the flow and experimental conditions are not the same in the two studies, and there is an effect of PKW in the upstream flow characteristics. Mostly, the rolling regime was observed over the upstream bed. Further, it was observed that particle moves in the inlet key while rolling over the key bed with intermittent small jumps. No saltation of the particle was observed in only three cases as shown in Table 3.

The proposed equation for obtaining the upstream shear stress

PKW geometry has a direct influence on the upstream flow condition and sediment movement. Therefore, it is necessary to analyze the correlation between PKW geometry, particle size and critical shear stress on the upstream bed required to pass sediment over inlet ($\boldsymbol{\tau_{cbik}}$). Out of the total of 36 collected datasets, 24 were used to establish a relationship of $\boldsymbol{\tau_{cbik}}$ with the independent variables d

and length magnification ratio *L/W*, and the remaining 12 datasets were utilized for validation. After applying the least square technique, Eq. (5) was found, which is applicable for $2.3 \le L/W \le 4.9$, $1.7 \le d \le 6.3$ mm, $0.31 \le H/P \le 0.73$ and *a/b* around 1.2.

$$\boldsymbol{\tau}_{cbik} = 0.0706\,d - 0.0041\,d^2 + 0.0131(L/W) + 0.0447 \qquad (R^2 = 0.941;\ d \text{ in mm}) \qquad (5)$$

Figure 10(b) illustrates a comparison between the computed and observed $\boldsymbol{\tau}_{cbik}$ for both the datasets used in calibration and validation. The maximum absolute percentage error, mean absolute percentage error and root mean square error for the validated datasets are 7.06%, 4.08% and 0.0133, respectively, which are within a permissible range. A good number of points, 62.5% of calibration and 66.67% of validation lie within only ±5% error range which shows a respectable performance of Eq. (5). All datasets except one lie within the error range of ±10%.

Shear stress and particle kinematics in the inlet key

As mentioned earlier, CFD simulation was performed to analyze the spatial variation in the shear stress $\boldsymbol{\tau}_o$ acting on the inlet key. The shear stress values were computed along the inlet key bed at a distance of 0.005 m from the right wall of flume because the tracked sediment moved along a plane close to the sidewall of the flume. Figures 11(a–b) and 12 show the variation of $\boldsymbol{\tau}_o$ along the inlet key bed of the models. Although the shear stress $\boldsymbol{\tau}_o$ rose gradually in all three cases in the upstream part of the key, i.e. L_k upto 0.06–0.07 m, it was found more or less constant in the middle part of the key, i.e. L_k from 0.06–0.07 m to 0.15–0.17 m. However, a rapid enhancement in $\boldsymbol{\tau}_o$ observed in the downstream part of the key where the flow velocity is also higher due to vertical contraction.

Figure 12 shows the comparison between the three plots of $\boldsymbol{\tau}_o$ obtained from CFD simulations. It was found that $\boldsymbol{\tau}_o$ rises with an increase in *L/W* and reduction in inlet width *a* for L_k upto 0.15–0.17 m, but an opposite trend was observed in the downstream part of the key beyond $L_k \approx 0.15$–0.17 m. For the same discharge, the maximum $\boldsymbol{\tau}_o$ was found for PK_1 model. Further, it was found that PK_1 requires higher discharge (and a slightly higher approach flow velocity) to pass the same sediment than the other two models. Therefore, it is justified that the highest $\boldsymbol{v}_s$ and $\boldsymbol{a}_s$, as shown in Figs. 6(a–b), which were found in the downstream part of the key for PK_1 than other two models are due to the higher shear stress imposed in case of PK_1 for a particular d. Further, $\boldsymbol{v_s}$ and $\boldsymbol{a_s}$ increased quickly in the upstream part of the key for PK_3 model where a significant rise in $\boldsymbol{\tau_o}$ was found. The particle velocity did not increase much in the middle part of the key similarly to $\boldsymbol{\tau_o}$. There is a strong correlation between $\boldsymbol{\tau_o}$ and particle kinematics, and the assumption $\boldsymbol{a_s} = f(\boldsymbol{\tau_o})$ is acceptable.

Correlation between particle motion and flow characteristics

As the particle motion is closely related to the flow properties, the correlation between flow and sediment parameters were analyzed. Figure 13(a) shows different parameters related to the study. Upstream flow velocity $\boldsymbol{V_c}$ and Froude number Fr were calculated at 0.5 m upstream of the outlet key, whereas the maximum particle velocity $\boldsymbol{v_{s\,max}}$ was obtained from particle movements. The mean flow velocity at the downstream end of the key $\boldsymbol{V_{max}}$ could not be measured precisely using ADV probably due to high turbulence and unsteadiness in the flow and flow separation at the tip of the sensor, and therefore, CFD simulation was done for two discharges 16.1×10^{-3} and 18.45×10^{-3} m^3/s passing over PK_1. A larger particle needs higher $\boldsymbol{V_c}$ and Fr to travel. Interestingly, it was noticed that $\boldsymbol{v_{s\,max}}$ is much higher in case of PK_1 model as compared to others and it mostly increases with particle size. However, Fig. 13(b) depicts that such a trend was not observed for PK_2 and PK_3. The highest observed $\boldsymbol{v_{s\,max}}$ in the study was 0.617 m/s for PK_1. The flow recirculation and vortices inside the inlet key observed by Denys and Basson (2020) appear to be affecting the particle movement varying with the key width. Further, Fig. 12 shows that for a constant discharge the shear stress varied inversely with L/W at the downstream end of the inlet. While comparing the normalized maximum particle velocity $\boldsymbol{v_{s\,max}/V_c}$ to the normalized particle size d/y, a declining trend of $\boldsymbol{v_{s\,max}/V_c}$ was observed as shown in Fig. 13(c), even though $\boldsymbol{v_{s\,max}}$ increases with particle size for PK_1. Thus, $\boldsymbol{v_{s\,max}}$ increases at a slower rate than $\boldsymbol{V_c}$. Figure 13(d) shows that the enhancement of critical shear stress on the upstream bed is higher for smaller particles as compared to the larger ones. It was found that $\boldsymbol{\tau_{cbik}}$ is dominated more by d than L/W. Further, it was noticed for all particles that PK_3 requires much lower discharge to pass them than PK_1 and PK_2. Meanwhile, normalizing $\boldsymbol{\tau_{cbik}}$ by $\boldsymbol{\tau_{cbib}}$ it was found that about 17% to 43% of additional shear stress (except one result) is required upstream of PKW to move sediment over it. The average amount is being 31%. Figure 13(e) shows such variation with respect to d. When the discharge was compared, it was found that 1.08–1.31 (average 1.23) times discharge is required to move sediment over PKW than that of upstream bed. This additional shear stress is being utilized to counter the tangential component of the particle weight to move it over the slopping key. Finally, the ratio of $\boldsymbol{v_{s\,max}}$ to $\boldsymbol{V_{max}}$ obtained from CFD simulation of PK_1 is found to be 0.69 and 0.78 for 2.0 and 2.58 mm particles, respectively, which is close to the value ($\boldsymbol{v_{s\,max}}/\boldsymbol{V_{max}}$ = 0.73) found by Kumar et al. (2019) for movement of 2.18 mm particle over a ramp.

Conclusions

The particle motion parameters at critical sediment movement in the inlet key of three type-A PKW models were determined experimentally. It was observed that sediment generally slows down while moving from upstream towards the inlet key and mostly accelerates instantly after reaching near the key entrance. The accelerating flow pattern formed by the flow contraction attributes to such a phenomenon. The rolling and saltation regimes were observed over the inlet key and particle generally accelerates in the rising part of a saltation event and decelerates in its falling part. The observed angle of orientation of particle velocity vector to the horizontal axis, $\boldsymbol{\theta_s}$ varies from 50.9 to 13.8 degree, and its range is higher for PK_1 and generally proportionate to d. The rapid rotations of sediment during rolling and saltation regimes, its jumps during saltation and the irregularity in particle shape contribute to the fluctuation of $\boldsymbol{\theta_s}$. The distributions of $\boldsymbol{\theta'_s}$ and $\boldsymbol{a'_s}$ for all three models are nearly bell-shaped, but the distribution of $\boldsymbol{v'_s}$ for PK_2 and PK_3 does not follow such a trend. Further, it was observed that particle accelerates rapidly in upstream and downstream parts of the key, but the particle velocity did not increase much in the middle part. The maximum observed $\boldsymbol{v_s}$ values at the key end are 0.617, 0.609 and 0.458 m/s for PK_1, PK_2 and PK_3, respectively. The highest $\boldsymbol{v_s}$ and $\boldsymbol{a_s}$ values were witnessed for PK_1 having a wider inlet key and which requires higher discharge (and a slightly higher approach flow velocity) to pass sediment than the other two models. For the same discharge, the maximum $\boldsymbol{\tau_o}$ was found for PK_1 model. CFD simulation showed that $\boldsymbol{\tau_o}$ rises gradually in the upstream part of the key, stays more or less constant in the middle part and enhances rapidly in the downstream part. Hence, the particle kinematics is strongly influenced by $\boldsymbol{\tau_o}$ and the assumption $\boldsymbol{a_s} = f(\boldsymbol{\tau_o})$ is acceptable. However, the effect of variation in the basset force, especially for the smaller particles could influence the said assumption. For PK_1, the ratios of $\boldsymbol{v_{s\,max}}$ to $\boldsymbol{V_{max}}$ were obtained to be 0.69 and 0.78 for 2.0 and 2.58 mm particles, respectively. The proposed equation underestimated the Shields number (within a considerable range), perhaps due to different experimental conditions. Finally, for the used models, it was obtained that, additional shear stress amounting 17% to 43% is required to counter the tangential component of particle weight to move it over the slopping key. This study is an important addition to the recent developments on PKW and will be very useful in planning and hydraulic design of PKW as diversion structure keeping in mind the problem of upstream siltation.

However, the present investigation is limited to singular particle movements over the inlet key of type-A PKWs and the lateral component of particle movement in the approaching segment could not be determined due to 2D tracking. Further research may be carried out with different PKW types to relate the particle motion with the upstream flow condition affected by the PKW geometry and particularly by the obstruction caused by the outlet key overhangs. In addition to this, a study may also be carried out to identify the effect of the key slope which is related to the tangential component of the sediment weight.

Data Availability Statement

The supporting data which are associated with the findings of this study can be obtained from the corresponding author upon genuine request.

Acknowledgement

The first author is extremely thankful to the Ministry of Human Resource Development, Govt. of India for research scholarship.

Conflicts of interests

The authors do hereby declare that they do not have any conflict of interest.

References

Abbott, J. E., and Francis, J. R. D. (1977). “Saltation and Suspension Trajectories of Solid Grains in a Water Stream.” *Philosophical Transactions of the Royal Society A: Mathematical, Physical and*

Engineering Sciences, 284(1321), 225–254.

Abhash, A., and Pandey, K. K. (2020). "A review of Piano Key Weir as a superior alternative for dam rehabilitation A review of Piano Key Weir as a superior alternative for dam rehabilitation." *ISH Journal of Hydraulic Engineering*, 1–11.

Ancey, C., Bigillon, F., Frey, P., Lanier, J., and Ducret, R. (2002). "Saltating motion of a bead in a rapid water stream." *Physical Review*, E 66(036306), 1–16.

Anderson, R. M., and Tullis, B. P. (2013). "Piano Key Weir Hydraulics and Labyrinth Weir Comparison." *Journal of Irrigation and Drainage Engineering*, 139(3), 246–253.

ANSYS. (2018). "ANSYS Academic Research Mechanical and CFD, Release 19.1." Canonsburg, PA.

Bai, Y., and Duan, J. G. (2014). "Simulating unsteady flow and sediment transport in vegetated channel network." *Journal of Hydrology*, 515, 90–102.

Berggren, M., Ekström, S. E., and Nordström, J. (2009). "A discontinuous Galerkin extension of the vertex-centered edge-based finite volume method." *Communications in Computational Physics*, 5(2–4), 456–468.

Bombardelli, F. A., González, A. E., and Niño, Y. I. (2008). "Computation of the Particle Basset Force with a Fractional-Derivative Approach." *Journal of Hydraulic Engineering*, 134(10), 1513–1520.

Bridge, J. S., and Dominic, D. F. (1984). "Bed Load Grain Velocities and Sediment Transport Rates." *Water Resources Research*, 20(4), 476–490.

Carvalho, E., Maia, R., and Proença, M. F. (2010). "Shear Stress Measurements over Smooth and Rough Channel Beds." *Proc. of the River Flow 2010 Conference, Braunschweig, Germany*, 367–375.

Chien, N., and Wan, Z. (1999). *Mechanics of Sediment Transport*. American Society of Civil Engineers, Reston, VA.

Chiew, Y., and Parker, G. (1994). "Incipient sediment motion on non-horizontal slopes." *Journal of Hydraulic Research*, 32(5), 649–660.

Crookston, B. M., Anderson, R. M., and Tullis, B. P. (2018). "Free-flow discharge estimation method for Piano Key weir geometries." *Journal of Hydro-environment Research*, 19, 160–167.

Crookston, B. M., Erpicum, S., Tullis, B. P., and Laugier, F. (2019). "Hydraulics of Labyrinth and Piano Key Weirs: 100 Years of Prototype Structures, Advancements, and Future Research Needs." *Journal of Hydraulic Engineering*, 145(12), 02519004.

Das Singhal, G., and Sharma, N. (2011). "Rehabilitation of Sawara Kuddu Hydroelectric Project – Model studies of Piano KeyWeir in India." *Proceedings of the International Conference on Labyrinth and Piano Key Weirs -PKW 2011, Liege, Belgium*, CRC Press, London, 241–250.

Denys, F. J. M., and Basson, G. R. (2020). "Unsteady Hydrodynamic Behavior at Piano Key Weirs." *Journal of Hydraulic Engineering*, 146(5), 04020028.

Erpicum, S., Archambeau, P., Dewals, B., and Pirotton, M. (2017). "Hydraulics of Piano Key Weirs: A review." *Proceedings of the 3rd International Workshop on Labyrinth and Piano Key Weirs (PKW 2017), Qui Nhon, Vietnam*, CRC Press, London, 27–36.

Eslinger, K. R., and Crookston, B. M. (2020). "Energy Dissipation of Type a Piano Key Weirs." *Water*, 12(5), 1253.

Fan, J., and Morris, G. L. (1992). "Reservoir Sedimentation. I: Delta and Density Current Deposits." *Journal of Hydraulic Engineering*, 118(3), 354–369.

Fernandez Luque, R., and Van Beek, R. (1976). "Erosion and Transport of Bed-Load Sediment." *Journal of Hydraulic Research*, 14(2), 127–144.

Ferro, V. (2003). "ADV measurements of velocity distributions in a gravel-bed flume." *Earth Surface Processes and Landforms*, 28, 707–722.

Francis, J. R. D. (1973). "Experiments on the motion of solitary grains along the bed of a water-stream." *Proceedings of the Royal Society A: Mathematical, Physical and Engineering Sciences*, 332(1591), 443–471.

Garde, R. J., and Albertson, M. L. (1959). "Sand Waves and Regimes of Flow in Alluvial Channels." *IAHR, 8th Congress (Vol. 4)*, Montreal.

Garde, R. J., and Ranga Raju, K. G. (2015). *Mechanics of sediment transportation and alluvial stream problems*. Revised third edition. New Age International (P) Ltd., New Delhi.

Gebhardt, M., Herbst, J., Merkel, J., and Belzner, F. (2019). "Sedimentation at labyrinth weirs – an experimental study of the self-cleaning process." *Journal of Hydraulic Research*, 57(4), 579–590.

Ho Ta Khanh, M. (2017). "History and development of Piano KeyWeirs in Vietnam from 2004 to 2016." *Proceedings of the 3rd International Workshop on Labyrinth and Piano Key Weirs (PKW 2017), Qui Nhon, Vietnam*, CRC Press, London, 3–16.

Hu, H., Qian, Z., Yang, W., Hou, D., and Du, L. (2018). "Numerical study of characteristics and discharge capacity of piano key weirs." *Flow Measurement and Instrumentation*, 62, 27–32.

Jüstrich, S., Pfister, M., and Schleiss, A. J. (2016). "Mobile Riverbed Scour Downstream of a Piano Key Weir." *Journal of Hydraulic Engineering*, 142(11), 04016043.

Kadia, S., Kumar, B., and Ahmad, Z. (2020). "Discharge Characteristics of Triangular Weir with Upstream Ramp and Its CFD Modelling Using Ansys CFX Module." *Recent Trends in Environmental Hydraulics. GeoPlanet: Earth and Planetary Sciences*, M. B. Kalinowska, M. M. Mrokowska, and P. M. Rowiński, eds., Springer, Cham, 77–90.

Kumar, B., and Ahmad, Z. (2020). "Experimental study on scour downstream of a piano key weir with nose." *Proceedings of the 8th IAHR International Symposium on Hydraulic Structures ISHS2020*, R. Janssen and H. Chanson, eds., University of Queensland Library, Santiago, Chile.

Kumar, B., Kadia, S., and Ahmad, Z. (2019). "Experimental study of flow field and movement of sediment over a ramp." *Journal of Civil Engineering and Construction*, 8(2), 79–86.

Launder, B. E., and Spalding, D. B. (1972). *Lectures in mathematical models of turbulence*. Academic Press, London.

Launder, B. E., and Spalding, D. B. (1974). "The Numerical Computation of Turbulent Flows." *Computer Methods in Applied Mechanics and Engineering*, 3(1974), 269–289.

Lee, H., and Hsu, I. (1994). "Investigation of Saltating Particle Motions." *Journal of Hydraulic Engineering*, 120(7), 831–845.

Mazumder, B. S., Bhattacharyya, A., and Ojha, S. P. (2008). "Near-bed particle motion due to turbulent flow using image-processing technique." *Journal of Flow Visualization and Image Processing*, 15(1), 1–15.

Moreno-Casas, P. A., and Bombardelli, F. A. (2016). "Computation of the Basset force: recent advances and environmental flow applications." *Environmental Fluid Mechanics*, 16(1), 193–208.

Niño, Y., and García, M. (1994). "Gravel Saltation: 2. Modeling." *Water Resources Research*, 30(6), 1915–1924.

Niño, Y., and García, M. (1998a). "Using Lagrangian particle saltation observations for bedload sediment transport modelling." *Hydrological Processes*, 12(8), 1197–1218.

Niño, Y., and García, M. (1998b). "Experiments on Saltation of Sand in Water." *Journal of Hydraulic Engineering*, 124(10), 1014–1025.

Niño, Y., García, M., and Ayala, L. (1994). "Gravel saltation: 1. Experiments." *Water Resources Research*, 30(6), 1907–1914.

Noseda, M., Stojnic, I., Pfister, M., and Schleiss, A. J. (2019). "Upstream Erosion and Sediment Passage at Piano Key Weirs." *Journal of Hydraulic Engineering*, 145(8), 04019029.

Novak, P., and Nalluri, C. (1975). "Sediment transport in smooth fixed bed channels." *Journal of the Hydraulics Division*, 101(HY9), 1139–1154.

Novak, P., and Nalluri, C. (1984). "Incipient Motion of Sediment Particles over Fixed Beds." *Journal of Hydraulic Research*, 22(3), 181–187.

Oertel, M. (2018). "Piano Key Weir Research : State-of-the-art and Future Challenges." *7th IAHR International Symposium on Hydraulic Structures*, D. Bung and B. Tullis, eds., Utah State University, Aachen, Germany, 474–481.

Ramesh, B., Kothyari, U. C., and Murugesan, K. (2011). "Near-bed particle motion over transitionally-rough bed." *Journal of Hydraulic Research*, 49(6), 757–765.

Rostami, M., Ardeshir, A., Ahmadi, G., and Thomas, P. J. (2006). "Can the history force be neglected for the motion of particles at high subcritical Reynolds number range?" *International Journal of Engineering, Transactions B: Applications*, 19(1), 23–34.

Safari, M. J. S., Aksoy, H., Unal, N. E., and Mohammadi, M. (2017). "Experimental analysis of sediment incipient motion in rigid boundary open channels." *Environmental Fluid Mechanics*, 17(6), 1281–1298.

Schmeeckle, M. W., and Nelson, J. M. (2003). "Direct numerical simulation of bedload transport using a local, dynamic boundary condition." *Sedimentology*, 50(2), 279–301.

Sharma, N., and Tiwari, H. (2013). "Experimental study on vertical velocity and submergence depth near piano key weir." *Proceedings of the Second International Workshop on Labyrinth and Piano Key Weirs -PKW 2013*, CRC Press, London, 93–100.

Shields, I. A. (1936). *Anwendung der Aehnlichkeitsmechanik und der Turbulenzforschung auf die Geschiebebewegung. Mitteilungen der Pruessischen Versuchsanstalt für Wasserbau und Schiffbau*, Berlin [in German].

Shim, J., and Duan, J. (2019). "Experimental and theoretical study of bed load particle velocity." *Journal of Hydraulic Research*, 57(1), 62–74.

Shim, J., and Duan, J. G. (2017). "Experimental study of bed-load transport using particle motion tracking." *International Journal of Sediment Research*, 32(1), 73–81.

Silvestri, A., Archembeau, P., Pirotton, M., Dewals, B., and Erpicum, S. (2013). "Comparative analysis of the energy dissipation on a stepped spillway downstream of a piano key weir." *Proceedings of the Second International Workshop on Labyrinth and Piano Key Weirs -PKW 2013, Paris, France*, CRC Press, London, 111–120.

Tiwari, H., and Sharma, N. (2015). "Flow hydrodynamics near inlet key of Piano Key Weir (PKW)." *Sadhana*, 40(7), 2253–2261.

Tregnaghi, M., Bottacin-Busolin, A., Tait, S., and Marion, A. (2012). "Stochastic determination of entrainment risk in uniformly sized sediment beds at low transport stages: 2. Experiments." *Journal of Geophysical Research: Earth Surface*, 117(F4005), 1–17.

Voulgaris, G., and Trowbridge, J. H. (1998). "Evaluation of the Acoustic Doppler Velocimeter (ADV) for Turbulence Measurements." *Journal of Atmospheric and Oceanic Technology*, 15(1), 272–289.

Wiberg, P. L., and Smith, J. D. (1985). "A theoretical model for saltating grains in water." *Journal of Geophysical Research*, 90(C4), 7341–7354.

Zhao, C., Fang, H., Liu, Y., Dey, S., and He, G. (2020). "Impact of Particle Shape on Saltating Mode of Bedload Transport Sheared by Turbulent Flow." *Journal of Hydraulic Engineering*, 146(5), 04020034.

Notations

a = Inlet key width (m);

$\boldsymbol{a_s}$ = Resultant acceleration of sediment particle (m/s^2);

B = Sidewall overflowing crest length (m);

B_b = Footprint length (m);

B_i = Overhang length for the inlet key (m);

B_o = Overhang length for the outlet key (m);

b = Outlet key width (m);

d = Size of the sediment particle ($\times 10^{-3}$ m);

Fr = Froude number of the approach flow (-);

$\boldsymbol{F_s}$ = Resultant force on sediment particle ($\times 10^{-5}$ N);

$\boldsymbol{F_t}$ = total hydrodynamic force acting on the particle due to the combination of drag and lift ($\times 10^{-5}$ N)

k = Turbulent kinetic energy (kg-m^2/s^2);

L = Crest length of PKW (m);

L_k = Horizontal distance from the beginning of the inlet key (m);

$\mathrm{N_{sh}}$ = Shields number or Shields parameter (-);

P = Height of inlet (P_i) and outlet keys (P_o) (m);

$\mathrm{PK_1}$ = One-cycle Piano key weir model;

$\mathrm{PK_2}$ = Two-cycles Piano key weir model;

$\mathrm{PK_3}$ = Three-cycles Piano key weir model;

Q = Discharge ($\times 10^{-3}$ m^3/s);

Re^* = Particle Reynolds number (-);

$\mathrm{R_p}$ = Explicit particle Reynolds number (-);

$S_i = S_o$ = Slope of inlet and outlet keys (-);

S_s = Specific gravity of sediment (-);

T_s = Wall thickness (m);

$\boldsymbol{u_c^*}$ = Shear velocity (m/s);

$\boldsymbol{V_c}$ = Mean flow velocity at 0.5 m upstream of PKW (m/s);

$\boldsymbol{v_s}$ = Resultant velocity of sediment particle (m/s);

$\boldsymbol{v_{s\,max}}$ = Maximum resultant velocity of sediment particle (m/s);

$\boldsymbol{V_{max}}$ = Maximum flow velocity near the downstream weir drop (m/s);

W = Width of the weir (m);

$\boldsymbol{W'}$ = Submerged weight of the particle (N);

y = Depth of flow (m);

$\boldsymbol{\alpha}$ = Slope angle of the keys (degree);

γ = Specific weight of water (N/m^3);

ε = Turbulent kinetic energy dissipation rate (kg-m^2/s^3);

μ = Friction coefficient (-);

ν = Kinematic viscosity (m^2/s);

$\boldsymbol{\theta_s}$ = Angle of the orientation of particle velocity vector to the horizontal axis (degree);

$\boldsymbol{\tau_o}$ = Bed shear stress at any location on the inlet key (N/m^2);

$\boldsymbol{\tau_{cbib}}$ = Shear stress required to pass sediment over the upstream bed (N/m^2);

$\boldsymbol{\tau_{cbik}}$ = Shear stress required on the upstream bed to pass sediment over the inlet key bed (N/m^2).

List of Tables

Table 1. Summary of some valuable previous studies carried out on particle tracking during its movement over a fixed bed

Investigators	Experimental conditions	Contribution, observations
Francis (1973)	Fixed rough bed. Used multi-exposures photographs of individual particles taken at 40 frames per second (FPS). Different grain types ranging from 2.2 to 15.9 mm were used.	• Particle followed a low smooth trajectory in saltation regime and a wavy path in suspension regime due to irregular turbulence in the flow. • Saltation to suspension occurred when the vertical component of the turbulent velocity is close to the settling velocity.
Abbott and Francis (1977)	Used similar bed and photography conditions as Francis (1973). Different grain types from 6.4 to 8.8 mm were used.	• Obtained trajectories of single grain moving in rolling, saltation and suspension regimes. • The grains fall much gradually for low trajectories as compared to high trajectories and it is affected by the shear drift force.
Niño and García (1998b)	Fixed bed made with sand particles. Singular sand particles of size 0.5 mm were used for tracking using a high-speed video system at 250 FPS.	• Obtained the mean and standard deviation values of the streamwise particle velocity, saltation height and length. • The dimensionless saltation height is almost independent of *d*, but the dimensionless saltation length increased with *d*. • Collision-rebound type interactions between the saltation particle and fixed bed were observed.
Mazumder et al. (2008)	Rough bed condition. Used High-Speed Motion-Scope (HSMS) and digital image processing technique.	• Analyzed the instantaneous particle motion using forward difference technique and provided the basic equations to determine the particle kinematics parameters.

Table 1. (continued)

Investigators	Experimental conditions	Contribution, observations
Ramesh et al. (2011)	Transitionally rough fixed bed. Used a high-speed camera and image processing technique.	• Larger particles had a higher velocity in the rolling regime. As the density of particle reduced, it moved faster in saltation regime. • Bell-shaped distribution of the fluctuations in the angle of orientation of particle velocity vector and acceleration.
Kumar et al. (2019)	Tracking of movement of 2.18 mm particle over a ramp and smooth bed upstream of it using a high-speed camera.	• Increase in upward velocity along the ramp and particle accelerates towards the downstream end of the ramp. • Particle had very limited movement near the beginning of the ramp.

Table 2. Details of PKW configurations

Model	No. of cycles	L (m)	W (m)	P (m)	a (m)	b (m)	B_b (m)	$B_i = B_o$ (m)	$S_i = S_o$
PK_1	One	0.898			0.2	0.178			
PK_2	Two	1.402	0.39	0.105	0.1	0.083	0.125	0.064	5(V):9(H)
PK_3	Three	1.908			0.065	0.053			

Table 3. Regime of sediment at different locations during its incipient movement over the inlet key bed

Particle size, d (mm)	Shields number, N_{sh}			Regime as per Ancey et al. (2002)			Observed regime of sediment passing over Upstream bed			Observed regime of sediment passing over Inlet key bed		
	PK_1	PK_2	PK_3	PK_1	PK_2	PK_3	PK_1	PK_2	PK_3	PK_1	PK_2	PK_3
1.7	0.0056	0.007	0.0076	r	r	r	t, r	r	t, r	r, s	r, s	r, s
2.0	0.0065	0.0067	0.0075	r	r	r	r	r	t, r	r, s	r, s	r, s
2.18	0.0062	0.0063	0.0071	r	r	r	t, r	r	r	r, s	r, s	r
2.36	0.0062	0.0059	0.007	r	r	r	r	r	r	r, s	r, s	r, s
2.58	0.0057	0.0058	0.0067	r	r	r	t, r	r	r	r, s	r, s	r, s
2.8	0.0057	0.0055	0.0065	r	r	r	r	t	t	r, s	r, s	r, s
3.07	0.0056	0.0051	0.0061	r	r	r	r	r	t	r, s	r, s	r, s
3.35	0.0053	0.005	0.0057	r	t	r	t, r	r	t	r, s	r, s	r, s
4.05	0.0048	0.0043	0.0049	t	t	t	r	r	t	r, s	r, s	r, s
4.75	0.0043	0.0041	0.0045	t	t	t	r	r	r	r, s	r, s	r, s
5.5	0.0037	0.004	0.0042	t	t	t	t, r	r	r	r	r, s	r, s
6.3	0.0038	0.0038	0.0039	t	t	t	r	r	r	r	r, s	r, s

Note: t ≡ transition or sliding, r ≡ rolling, s ≡ saltation

Figure 1

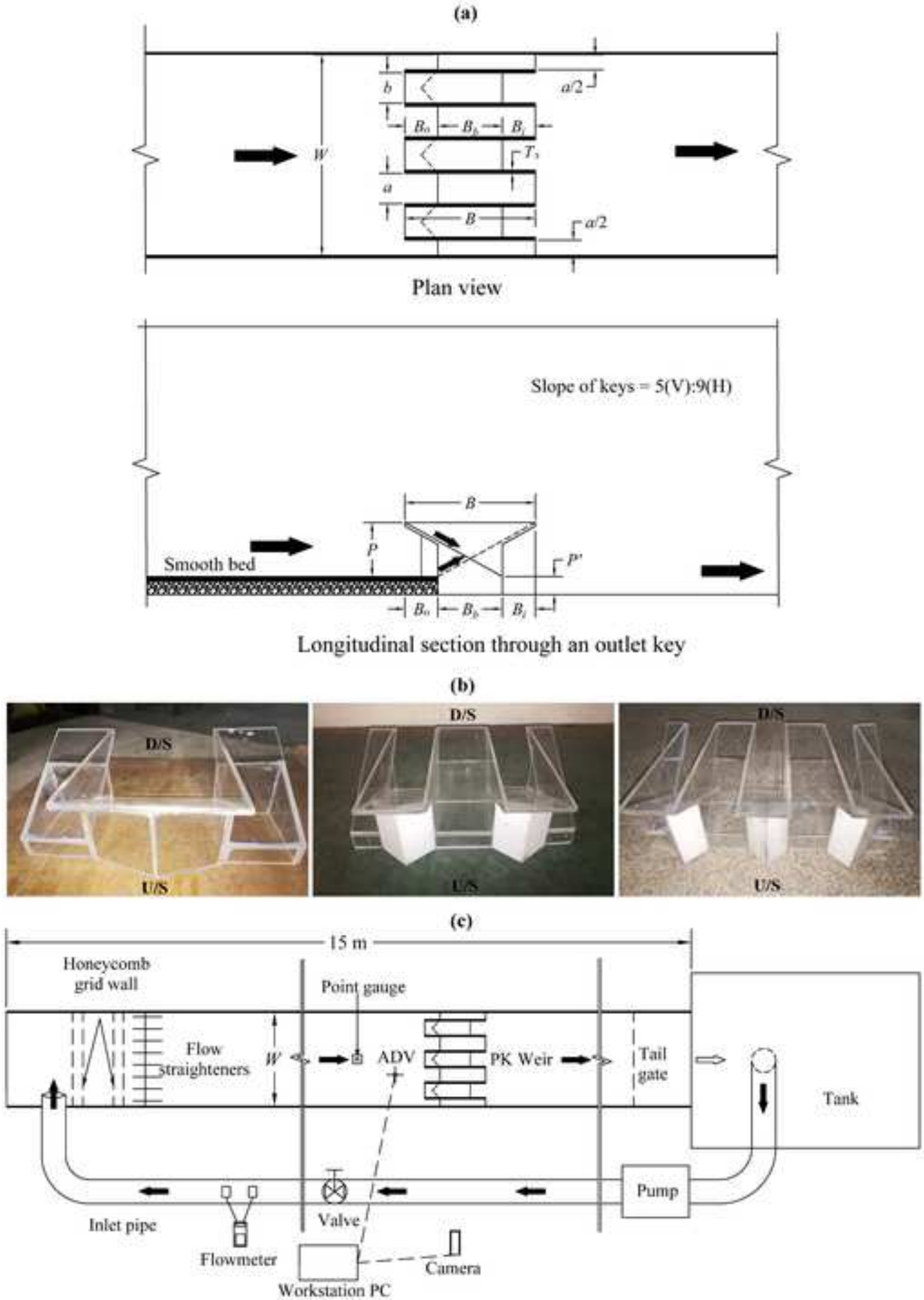
(a)
b
a/2
Bo
Bb
Bi
W
Ts
a
B
a/2
Plan view
Slope of keys = 5(V):9(H)
B
P
P'
Smooth bed
Bo
Bb
Bi
Longitudinal section through an outlet key
(b)
D/S
U/S
D/S
U/S
D/S
U/S
(c)
15 m
Honeycomb grid wall
Point gauge
Flow straighteners
W
ADV
PK Weir
Tail gate
Tank
Pump
Valve
Inlet pipe
Flowmeter
Workstation PC
Camera

Figure 2

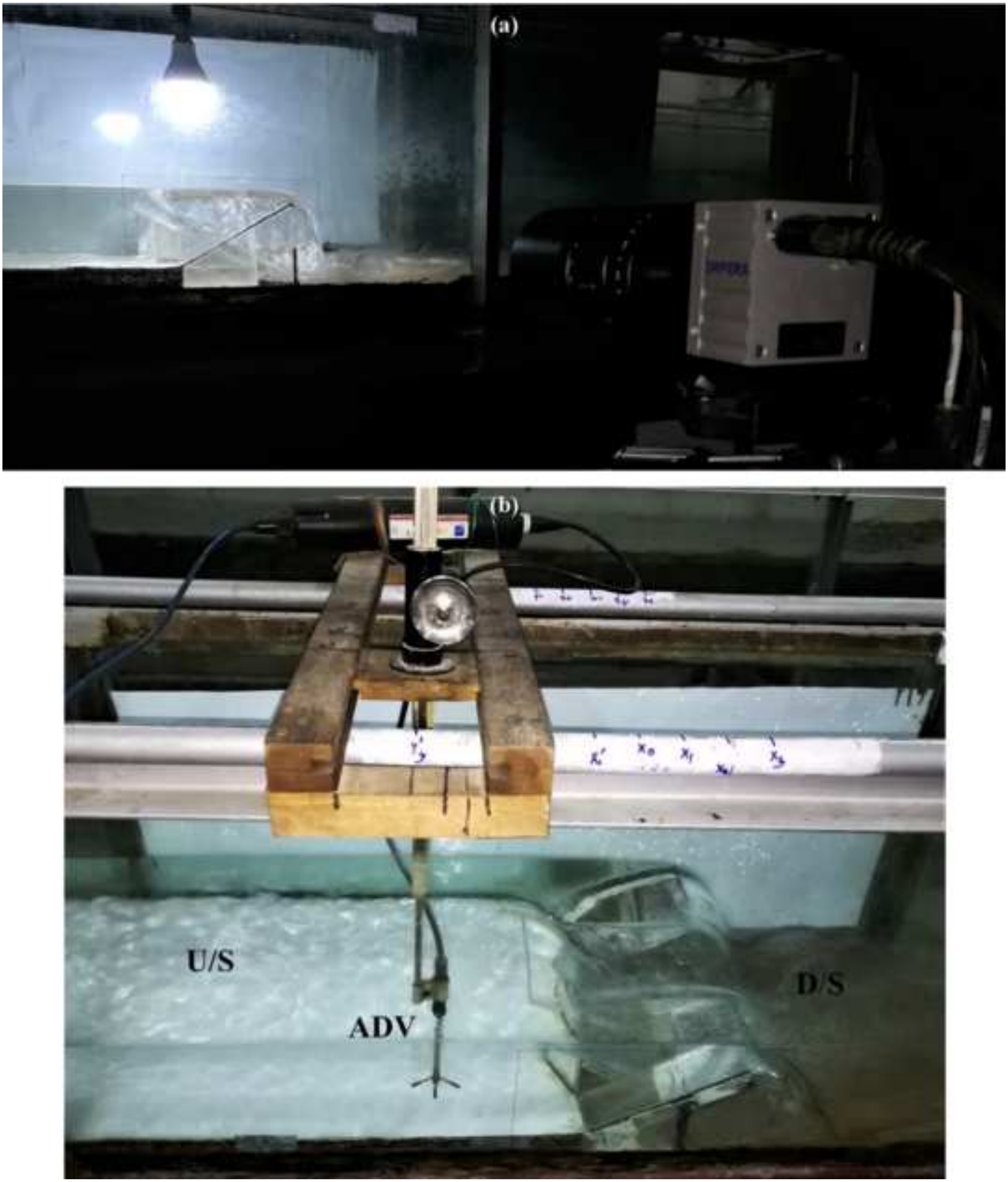

Figure 3

Click here to access/download;Figure;Fig. 3..tif

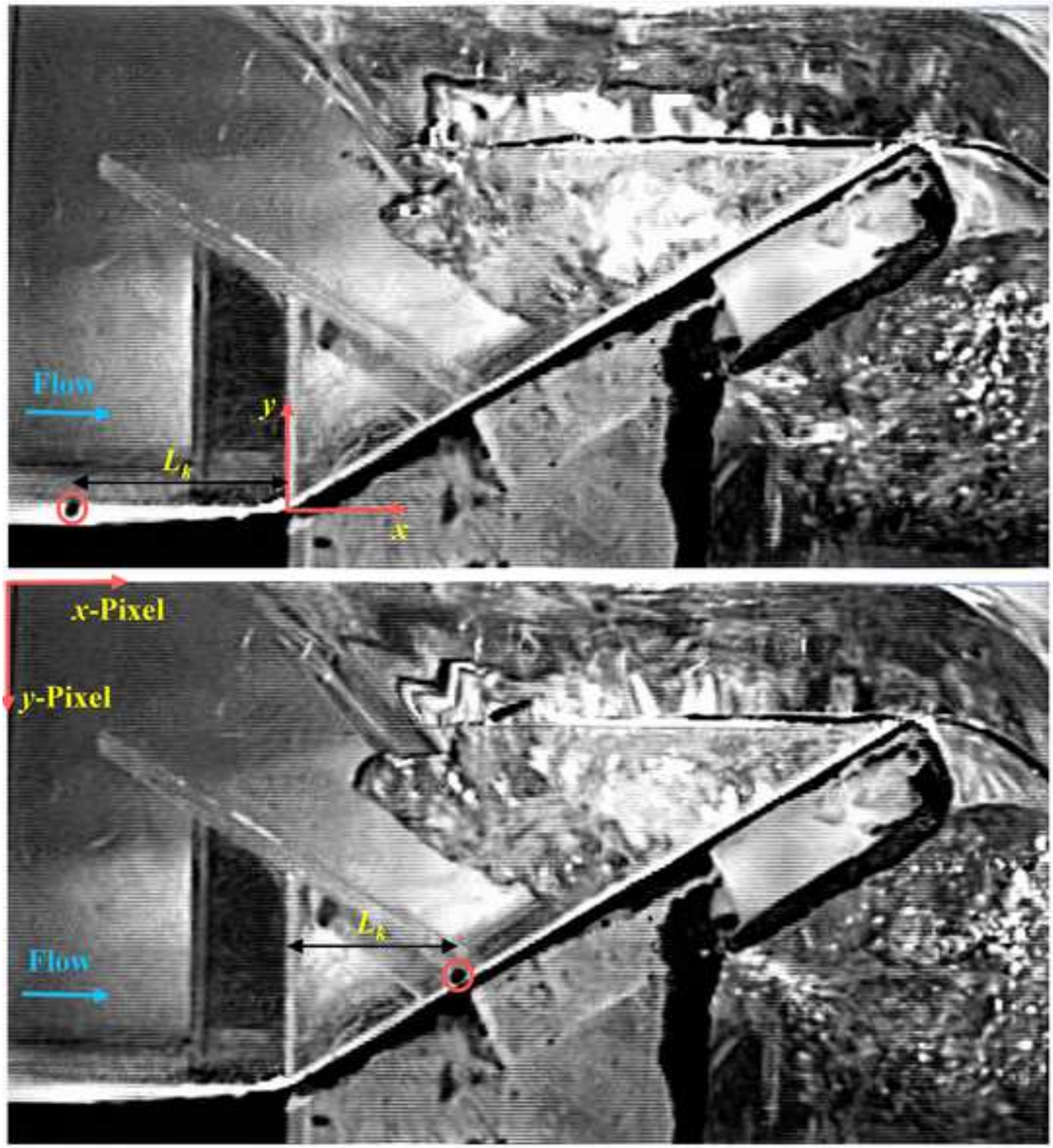

Figure 4

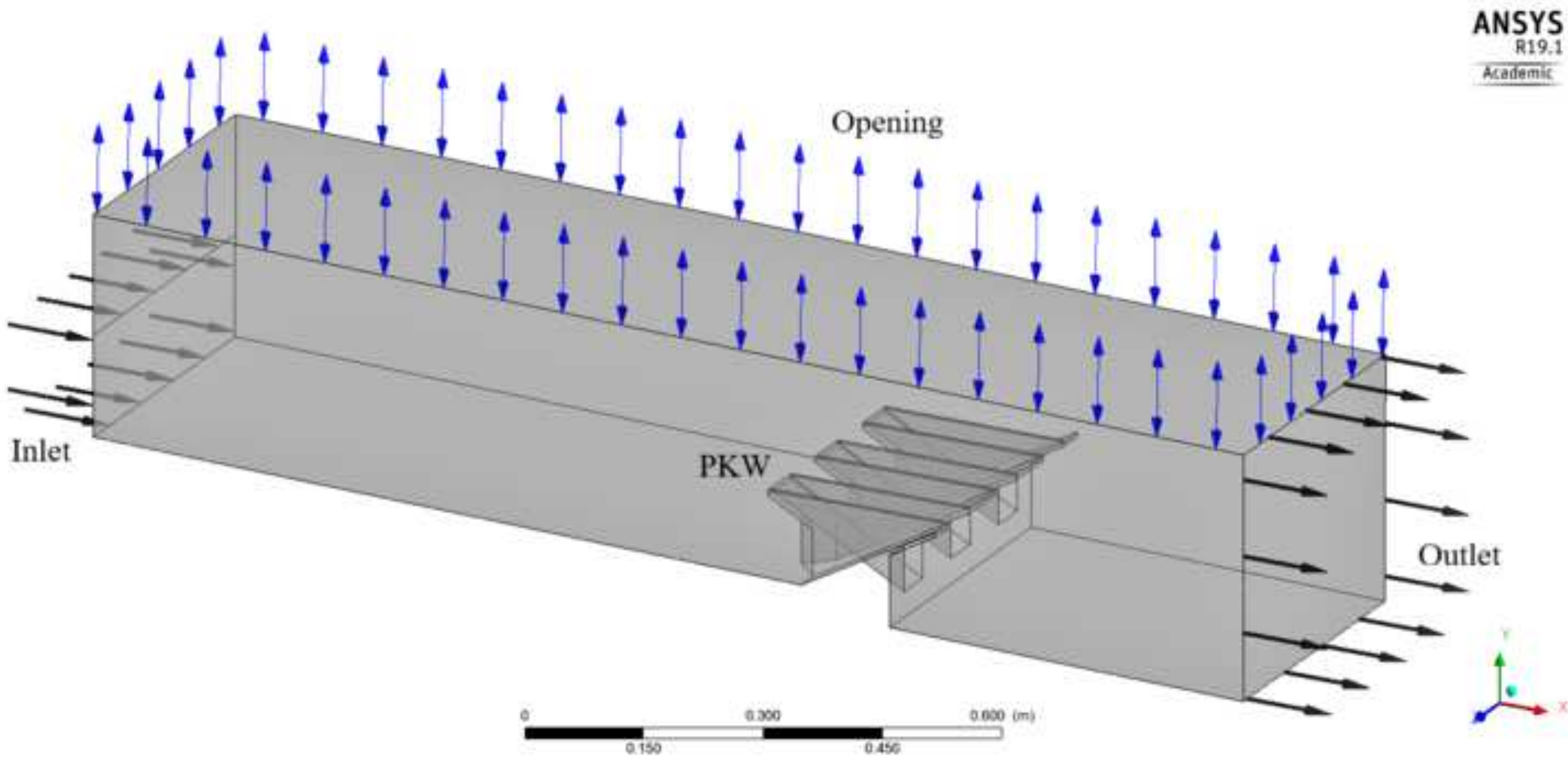

ANSYS
R19.1
Academic
Opening
Inlet
PKW
Outlet
0
0.300
0.600 (m)
0.150
0.450
Y
X

Figure 5

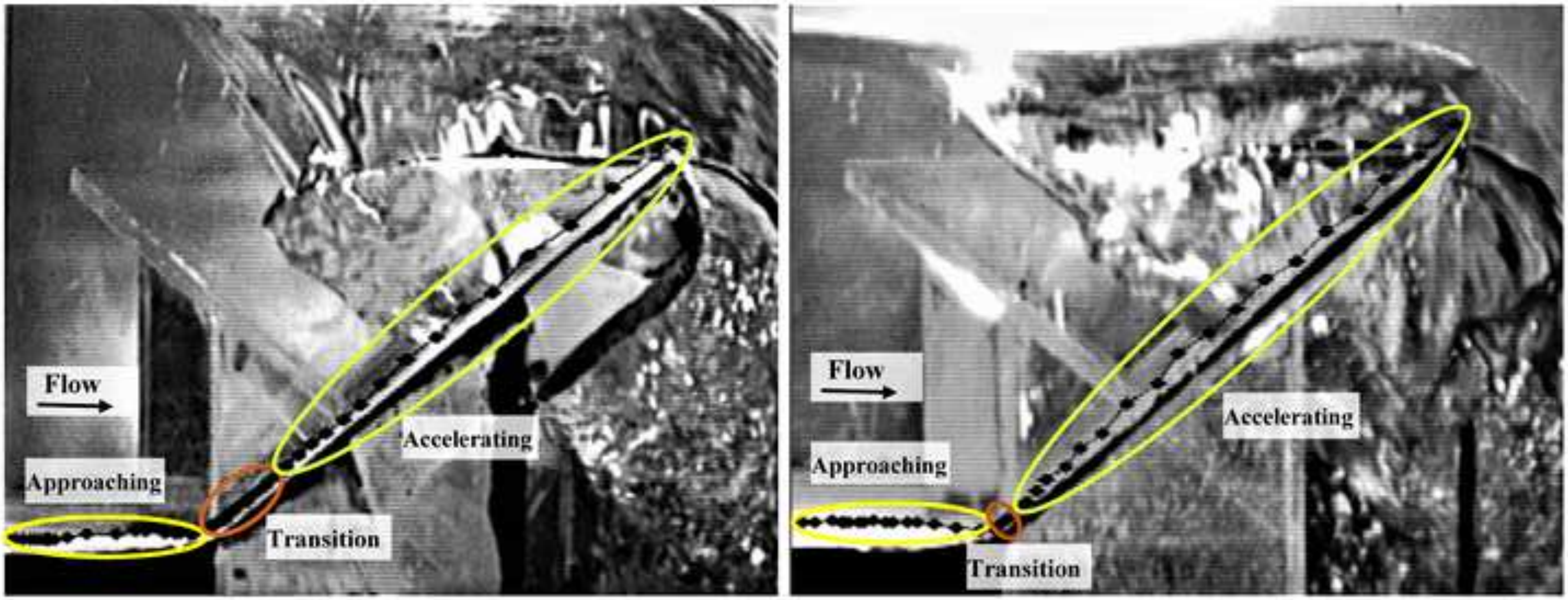
Flow
Approaching
Transition
Accelerating
Flow
Approaching
Transition
Accelerating

Figure 6 Click here to access/download;Figure;Fig. 6..tiff

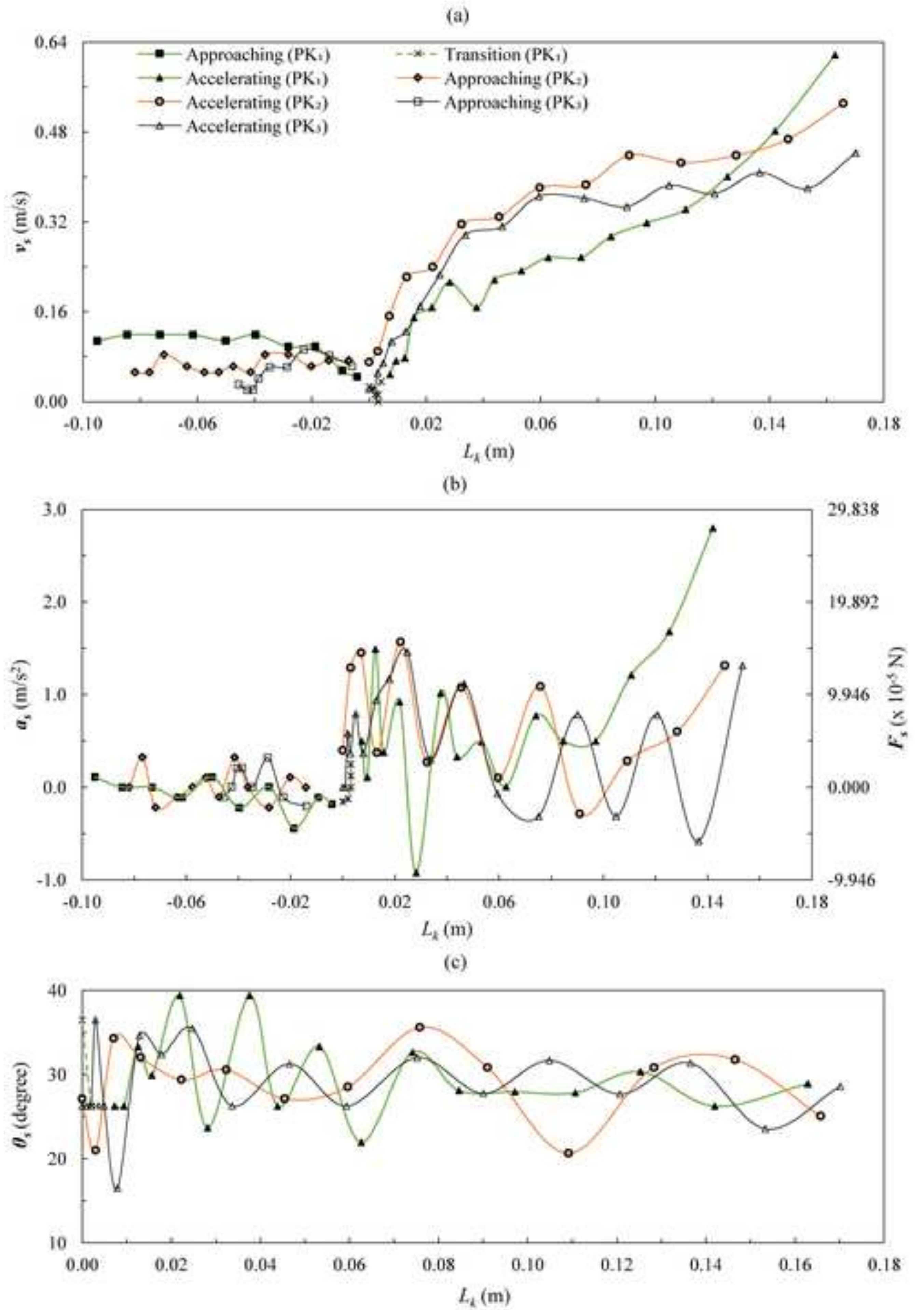

Figure 7

Click here to access/download;Figure;Fig. 7..tiff

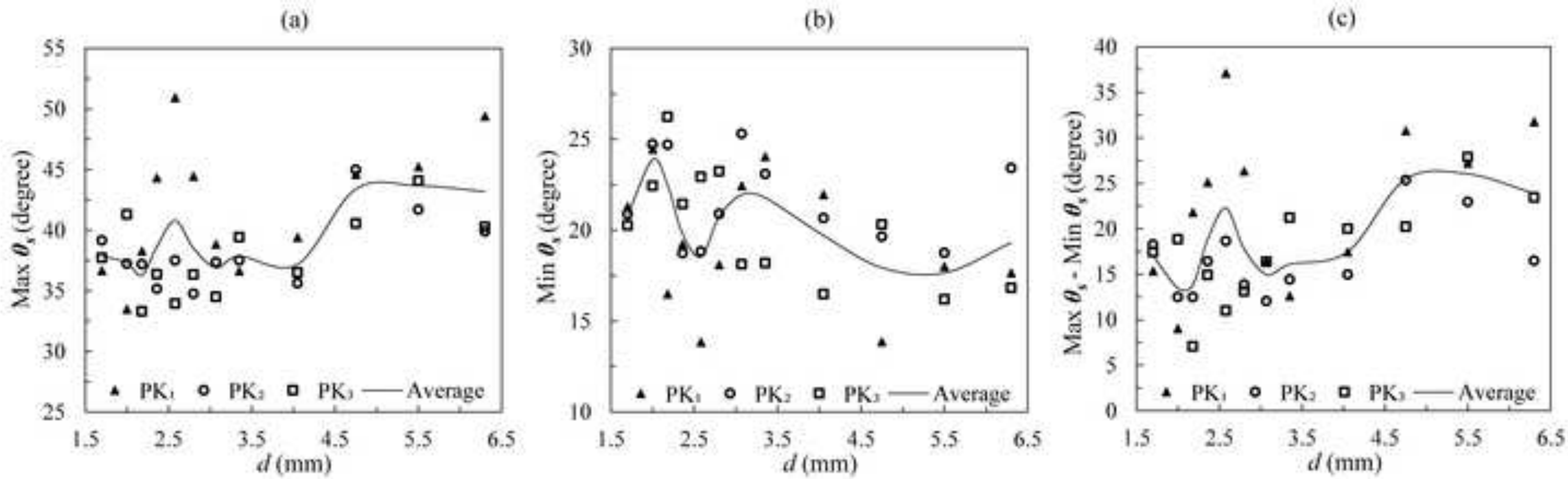

Figure 8

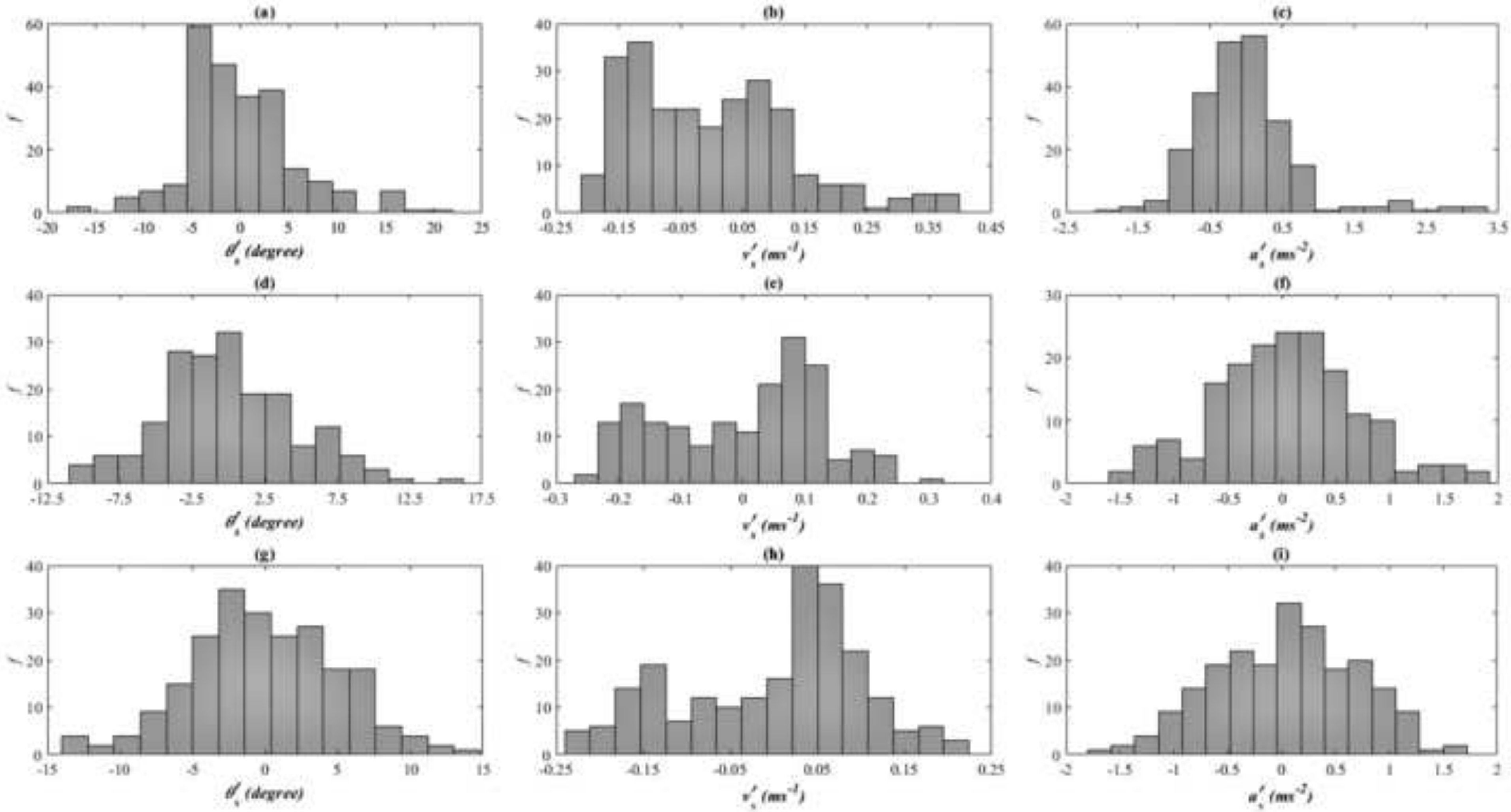

Figure 9

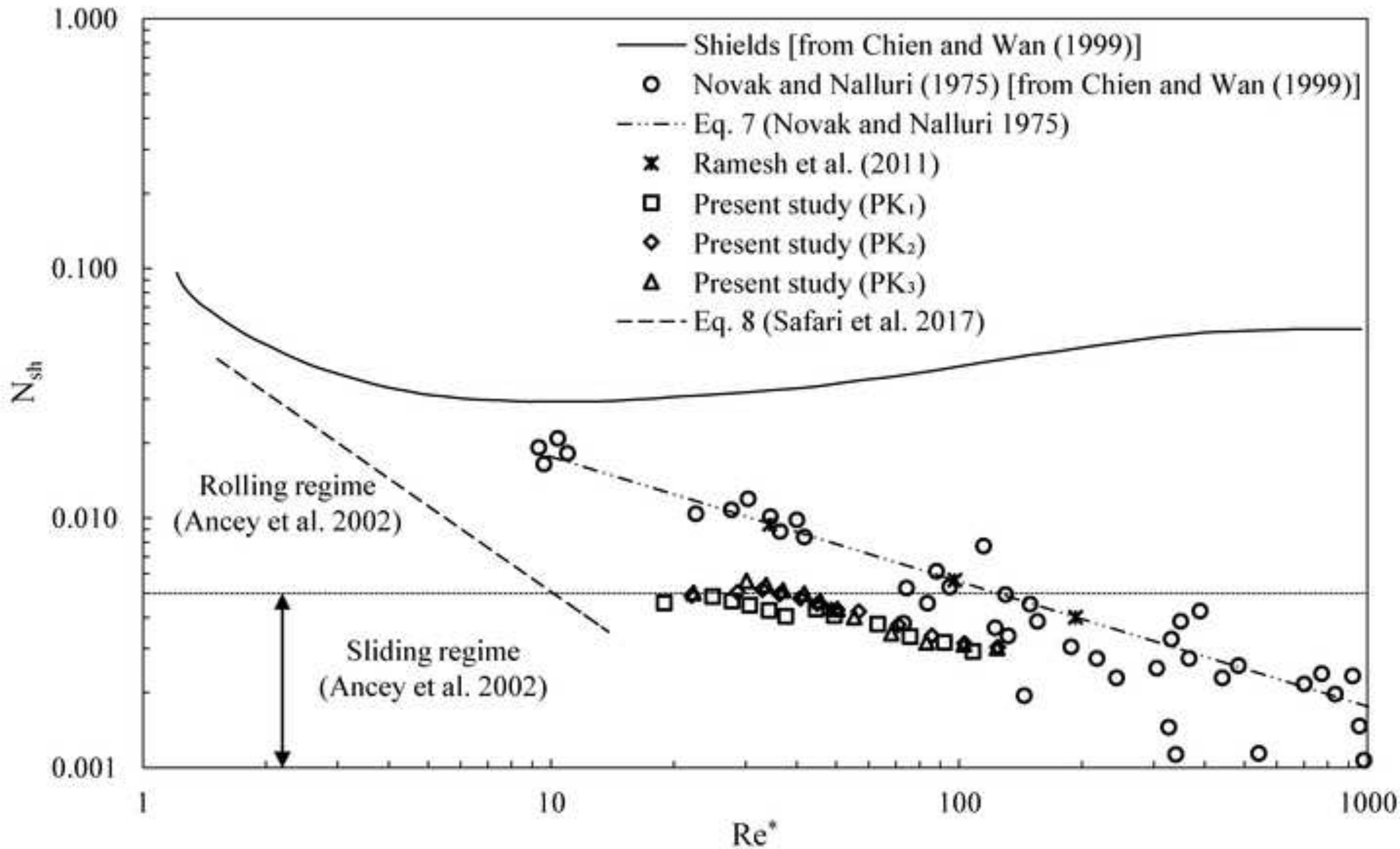

1.000
0.100
0.010
0.001
1
10
100
1000
N_sh
Re*
Shields [from Chien and Wan (1999)]
Novak and Nalluri (1975) [from Chien and Wan (1999)]
Eq. 7 (Novak and Nalluri 1975)
Ramesh et al. (2011)
Present study (PK1)
Present study (PK2)
Present study (PK3)
Eq. 8 (Safari et al. 2017)
Rolling regime
(Ancey et al. 2002)
Sliding regime
(Ancey et al. 2002)

Figure 10

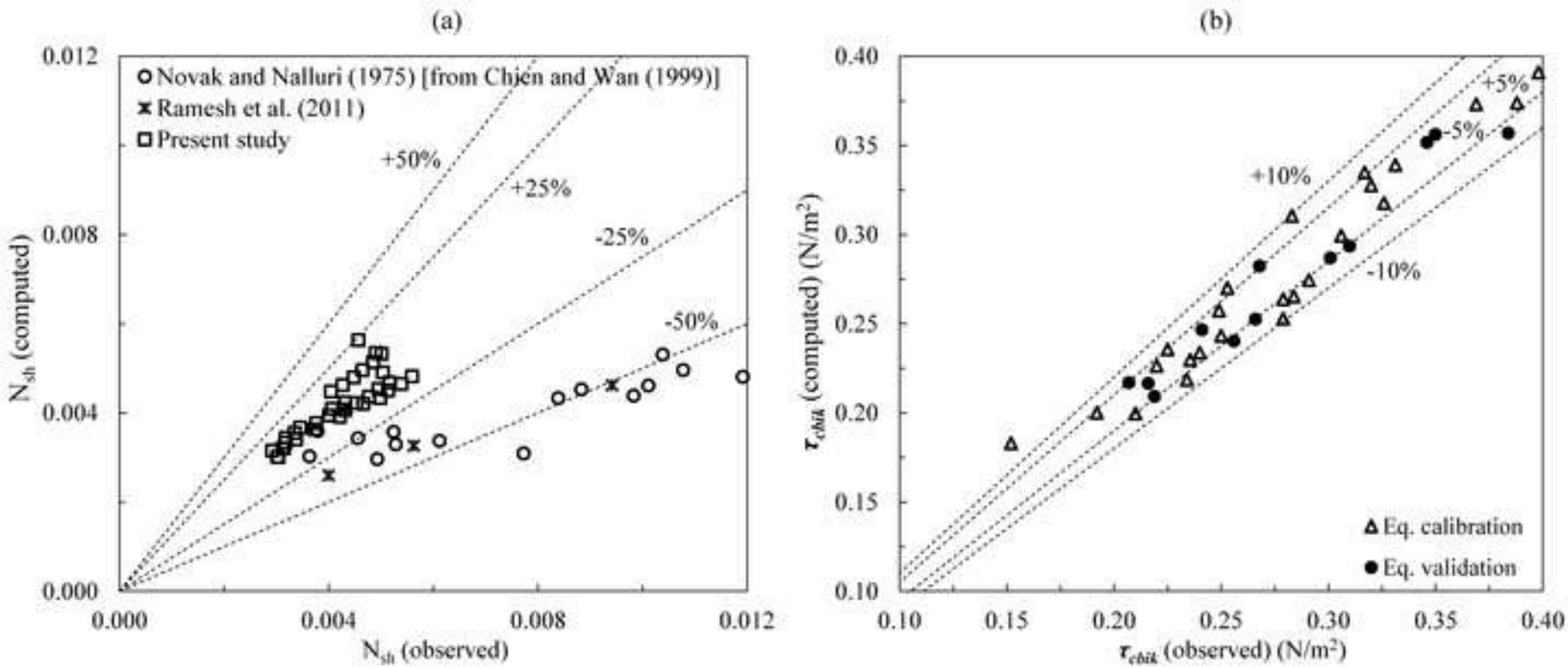
(a)
Novak and Nalluri (1975) [from Chien and Wan (1999)]
Ramesh et al. (2011)
Present study
+50%
+25%
-25%
-50%
0.012
0.008
0.004
0.000
0.000
0.004
0.008
0.012
N_{sh} (computed)
N_{sh} (observed)
(b)
+5%
-5%
+10%
-10%
Eq. calibration
Eq. validation
0.40
0.35
0.30
0.25
0.20
0.15
0.10
0.10
0.15
0.20
0.25
0.30
0.35
0.40
τ_{cbik} (computed) (N/m^2)
τ_{cbik} (observed) (N/m^2)

Figure 11

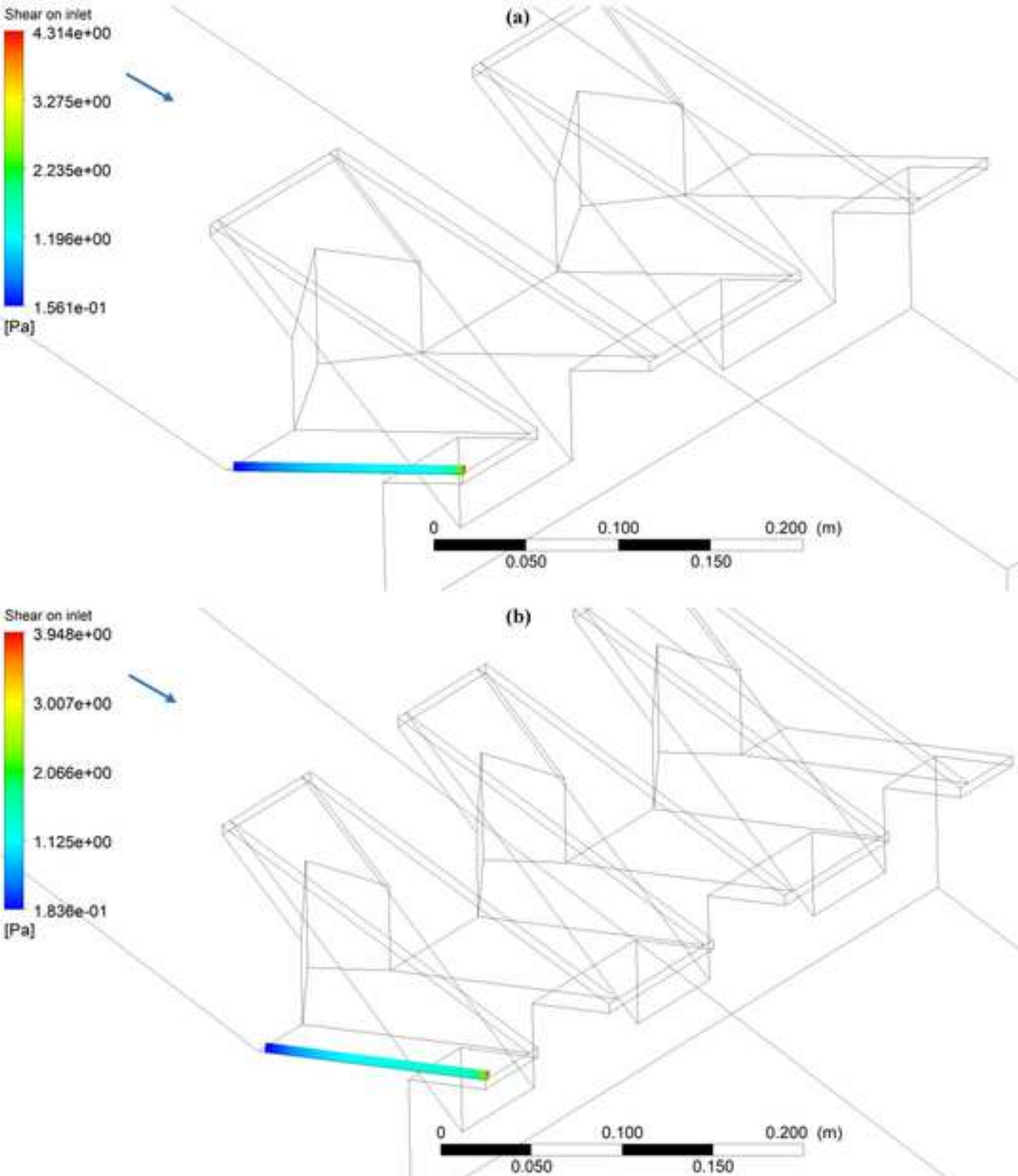
(a)
Shear on inlet
4.314e+00
3.275e+00
2.235e+00
1.196e+00
1.561e-01
[Pa]
0
0.100
0.200 (m)
0.050
0.150
(b)
Shear on inlet
3.948e+00
3.007e+00
2.066e+00
1.125e+00
1.836e-01
[Pa]
0
0.100
0.200 (m)
0.050
0.150

Figure 12

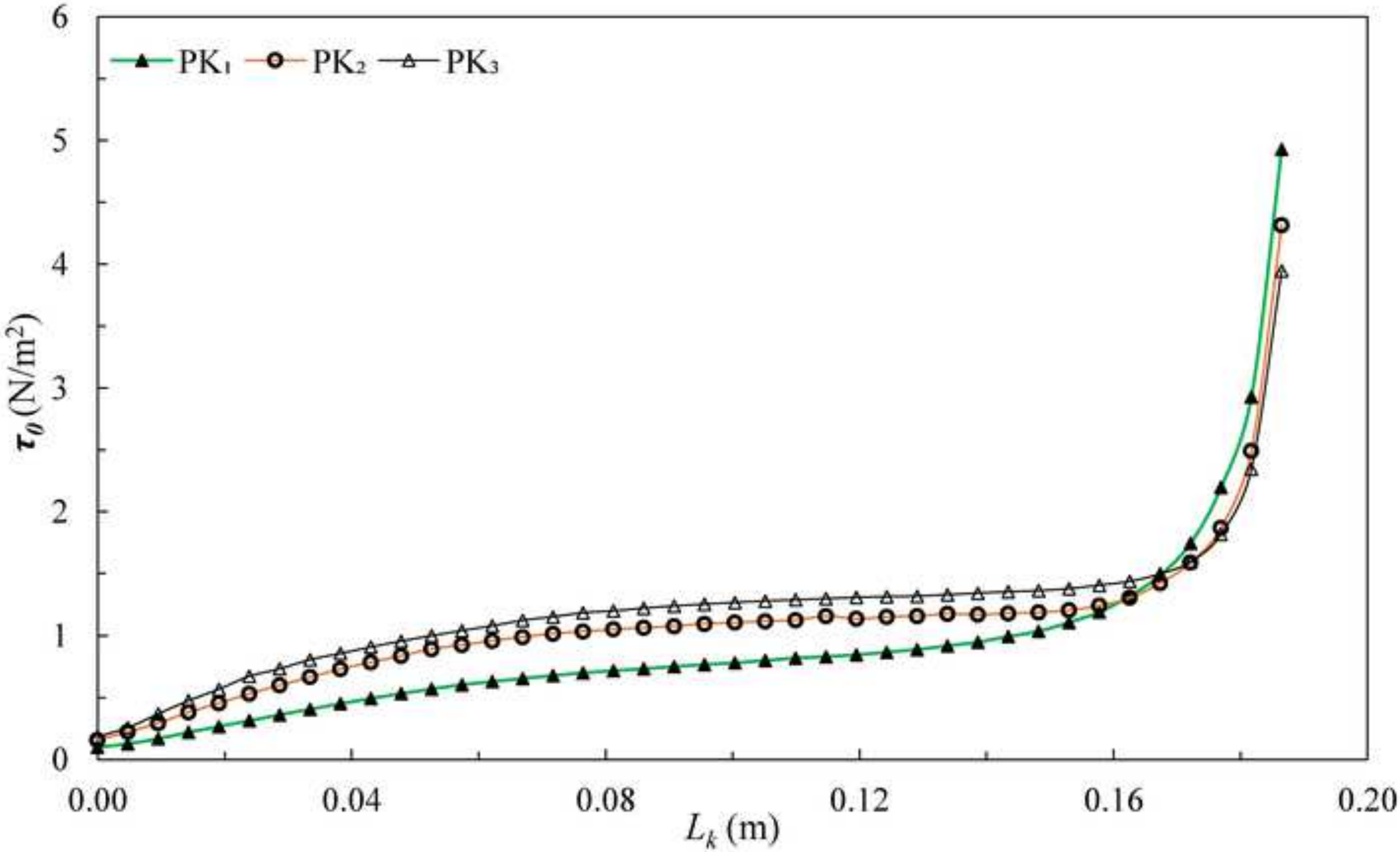

Figure 13 Click here to access/download;Figure;Fig. 13..tiff

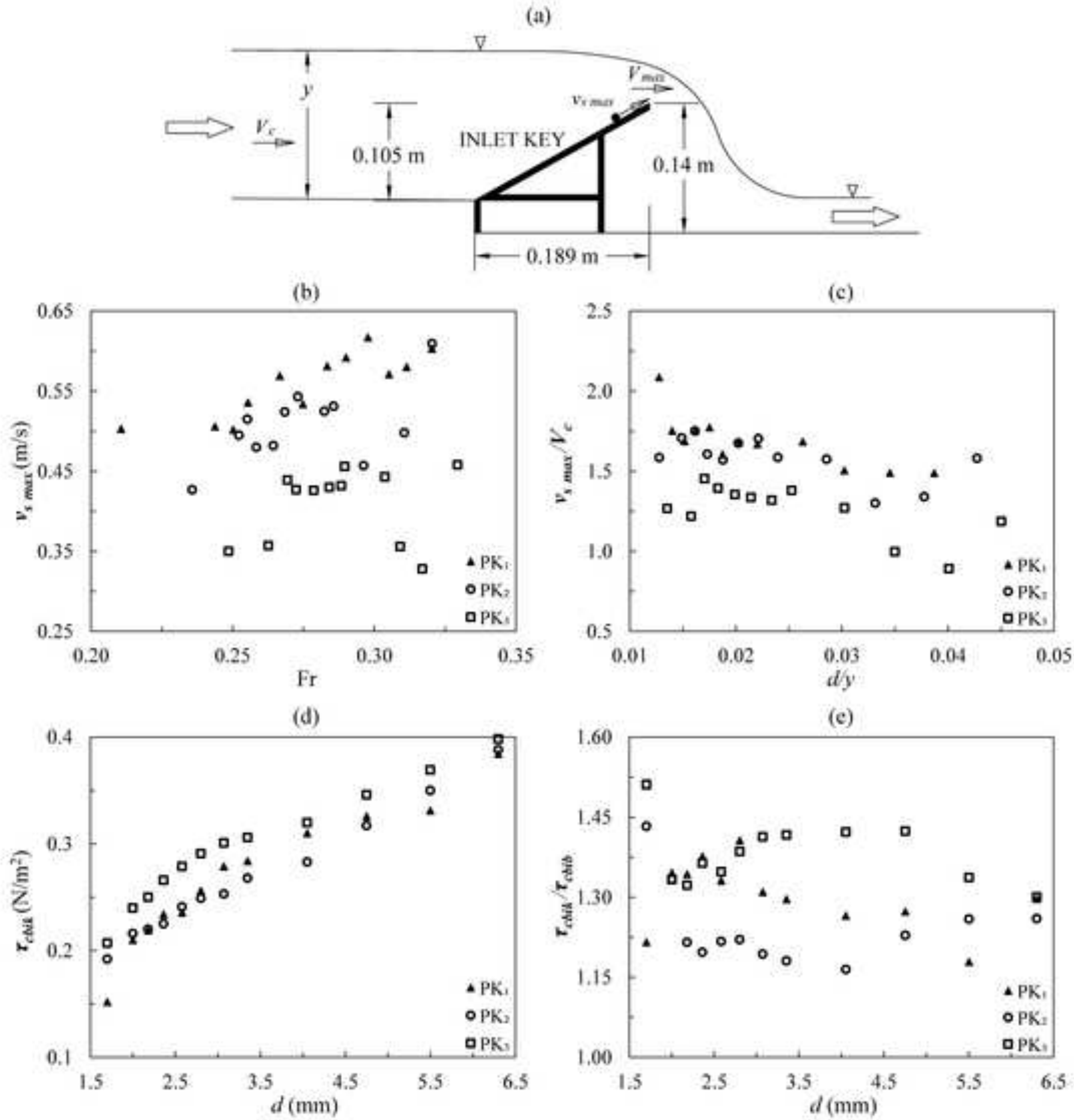

List of Figures